Journal of Materials Chemistry A

Accepted Manuscript

ROYAL SOCIETY OF CHEMISTRY

www.rsc.org/materialsA

Spray-printed CNT/P3HT organic thermoelectric film and power generator†

Cheon Taek Hong,‡[ab] Young Hun Kang,‡[a] Juwhan Ryu,[b] Song Yun Cho*[a] and Kwang-Suk Jang*[a]

[a]*Division of Advanced Materials, Korea Research Institute of Chemical Technology, Daejeon 34114, Republic of Korea. E-mail: kjang@krict.re.kr; scho@krict.re.kr*

[b]*Department of Polymer Science and Engineering, Chungnam National University, Daejeon 34134, Republic of Korea*

†Electronic supplementary information (ESI) available.

‡These authors equally contributed.

Abstract

This study demonstrates the fabrication of high-performance thermoelectric carbon nanotube /poly(3-hexylthiophene) (CNT/P3HT) nanocomposite films and flexible CNT/P3HT organic thermoelectric generators (OTEGs) by spray-printing. The spray-printed few-walled CNT/P3HT nanocomposite films exhibited excellent thermoelectric properties. The Seebeck coefficient, electrical conductivity, and power factor of the nanocomposite films were 97 ± 11 μV K^{-1}, 345 ± 88 S cm^{-1}, and 325 ± 101 μW $m^{-1}K^{-2}$, respectively, at room temperature. We fabricated the flexible OTEG solely from p-type CNT/P3HT nanocomposite patterns spray-printed on a polyimide substrate, and confirmed its electric power generation capabilities.

Main text

Thermoelectric materials have been studied extensively as clean energy-conversion materials. The performance of thermoelectric materials can be assessed by the figure of merit, $ZT = S^2\sigma T/\kappa$, where S, σ, T, and κ are the Seebeck coefficient, the electrical conductivity, the absolute temperature, and the thermal conductivity, respectively. As an alternative to the figure of merit, the power factor, $S^2\sigma$, is occasionally used because precise measurement of the in-plane thermal conductivity of a film on a substrate is difficult. Recently, organic thermoelectric materials have attracted much attention because of their potential for use in flexible, light weight, and low-cost printed organic thermoelectric generators (OTEGs).[1-17] Of the various organic thermoelectric materials currently available, films of conjugated polymers such as poly(3,4-ethylenedioxythiophene) (PEDOT), polyaniline (PANI) and poly(3-hexylthiophene) (P3HT) have been the most widely studied. However, the thermoelectric performance of conjugated polymer films needs to be further improved for application to

OTEGs. Recently, researchers have found that carbon nanotubes (CNTs) are effective fillers for enhancing the thermoelectric performance of conjugated polymer matrices.[3-17] Grunlan *et al.* reported that vacuum-filtrated single-walled CNT/PEDOT:poly(styrene sulfonate) (PSS) nanocomposite films exhibited power factors of up to 140 μW $m^{-1}K^{-2}$ at room temperature.[3] Müller *et al.* reported that drop-cast single-walled CNT/P3HT nanocomposite films exhibited power factors of 95 ± 12 μW $m^{-1}K^{-2}$ at room temperature.[4] Chen *et al.* reported that drop-cast single-walled CNT/PANI nanocomposite films exhibited power factors of up to 176 μW $m^{-1}K^{-2}$ at room temperature.[5] Yu *et al.* reported that drop-cast double-walled CNT/PANI nanocomposite films exhibited power factors of ~220 μW $m^{-1}K^{-2}$ at room temperature.[6] In another work, we reported that wire-bar-coated single-walled CNT/P3HT nanocomposite films exhibited power factors of 267 ± 38 μW $m^{-1}K^{-2}$ at room temperature.[7] Thermoelectric CNT/conjugated polymer nanocomposite films have been fabricated by solution-processing methods, such as drop-casting and bar-coating. However, such solution-processing techniques are not suitable for application to low-cost printed OTEGs, because additional processes are required for creating patterned organic thermoelectric materials on the substrates. Post-patterning processes are not compatible with continuous processes such as roll-to-roll printing; thus, research efforts are needed on the forming of the patterns of organic thermoelectric materials directly onto their substrates. For all their importance, there is a lack of research on printed thermoelectric CNT/conjugated polymer nanocomposites.

In this study, we report the high-performance characteristics of thermoelectric CNT/P3HT nanocomposite films created by the spray-printing process, and demonstrate the fabrication of a spray-printed flexible CNT/P3HT OTEG. Spray-printed CNT/P3HT nanocomposite films exhibited average power factors of 325 μW $m^{-1}K^{-2}$, which is the highest value of all thermoelectric CNT/conjugated polymers. We fabricated the flexible OTEG solely from p-

type CNT/P3HT nanocomposite patterns spray-printed on a polyimide substrate, and confirmed the electric power generation capabilities of the OTEG. To the best of our knowledge, spray-printed organic thermoelectric films and OTEGs have not yet been reported in the literature. Our results suggest that the spray-printing method is a promising candidate for the fabrication of flexible, light weight, and low-cost printed OTEGs.

To prepare the ink for thermoelectric CNT/P3HT nanocomposite films, a mixture of few-walled CNTs and P3HT in chloroform was sonicated in an ice bath. We used undoped P3HT with an electrical conductivity of ~10^{-5} S cm^{-1}. Only the absorbance for the neutral form (λ_{max} = 520 nm) was observed, and the absorbance for the oxidized form (λ_{max} = 800 nm) was not observed in the UV-vis spectrum of the P3HT film (Fig. S1). Janáky *et al*. reported that the slightly doped P3HT film exhibited electrical conductivity of ~10^{-5} S cm^{-1} and power factor of ~10^{-3} μW $m^{-1}K^{-2}$.[18] Although the electrical conductivity of P3HT is low for thermoelectric applications, the use of P3HT is advantageous for dispersion of CNTs. It was previously reported that the strong π-π interaction between CNT and P3HT leads to well-dispersed CNTs in a good solvent for P3HT, such as chloroform and *o*-dichlorobenzene.[7,17,19,20] Fig. S2 shows the UV-vis spectra of the CNT/P3HT ink with 50 wt% CNTs, CNT dispersion in chloroform, and P3HT solution in chloroform. The CNT dispersion showed no characteristic peaks. The absorbance peak of the P3HT solution at 450 nm is a characteristic peak of unstacked P3HT chains in the solution.[20,21] The absorbance peaks of the CNT/P3HT ink centered at 575 and 620 nm is assigned to the π-π stacked P3HT chains.[20-22] The red shift indicates π-π interaction between CNT and P3HT in the ink. The CNT bundles might be wrapped by the P3HT chains, resulting in an increase in the dispersion stability of the CNT/P3HT ink. To optimize the thermoelectric properties of the few-walled CNT/P3HT nanocomposites by varying the quantity of CNTs, we fabricated the nanocomposite films by drop-casting. While using ink

with more than 60 wt% CNTs, the drop-cast nanocomposite films were not uniform owing to the poor dispersion of CNTs in the ink. Thus, we prepared CNT/P3HT nanocomposite films with 20, 30, 40, and 50 wt% CNTs. The thickness of the CNT/P3HT nanocomposite films was 1.1 – 1.5 μm. No dependence of the film thickness on the quantity of CNTs was found. The CNT composition-dependent Seebeck coefficient, electrical conductivity, and power factor of the nanocomposite films were measured, as shown in Fig. 1. The Seebeck coefficients of the nanocomposite films were measured under dark ambient conditions utilizing a custom-built system. The Seebeck coefficient was obtained from the slope of the straight line fit of $\Delta V/\Delta T$.[7] The nanocomposite films exhibited positive Seebeck coefficient values, because of the p-type characteristics of both the CNTs and the P3HT. As the quantity of CNTs increases, the Seebeck coefficient decreases and the electrical conductivity increases. The power factor, calculated from the Seebeck coefficient and electrical conductivity, increases as the quantity of CNTs increases. The increase in the power factor originates from the large increase in the electrical conductivity of the nanocomposite film. As the quantity of CNTs increases, the density of the inter-CNT bundle connections in the nanocomposite films is expected to increase. The Seebeck coefficient, electrical conductivity, and power factor of nanocomposite films with 50 wt% CNTs were 102 ± 3 μV K^{-1}, 224 ± 19 S cm^{-1}, and 231 ± 19 μW $m^{-1}K^{-2}$, respectively, at room temperature. Because of the limitation in precise measurement of the in-plane thermal conductivity of a film on a substrate, the thermal conductivities of the nanocomposite films were not measured. In general, the thermal conductivity, κ, of materials is expressed as a sum of the electronic thermal conductivity, κ_e, and the lattice thermal conductivity, κ_l ($\kappa = \kappa_e + \kappa_l$). Although we cannot estimate the total in-plane thermal conductivity of the nanocomposite films, it is expected that the lattice thermal conductivity of the nanocomposite films can be reduced because of the blockage of phonon transport through interfaces between the nanostructured components.[4,8,9,23,24]

Figs. 2a and 2b show the atomic force microscope (AFM) and scanning electron microscope (SEM) images of the drop-cast CNT/P3HT nanocomposite film with 50 wt% CNTs. The network of CNT bundles with diameters in the range of 15 – 50 nm is clearly visible in the nanocomposite film. Because many P3HT chains are expected to wrap the surface of CNT bundles, the P3HT matrix cannot be identified individually. Because the electrical conductivity of CNT bundles is much higher than the polymer matrix, the resistance between the CNT bundles is a dominant factor in determining the electrical conductivity of the nanocomposite films.[4,7,25] Kymakis and Amaratunga reported the electrical conduction mechanism of CNT/non-conductive polymer nanocomposite films.[26] The electrical conduction in single-walled CNT films followed a three-dimensional variable-range hopping model, while that in the CNT/polymer nanocomposite films with CNT compositions less than 35 wt% obeyed a fluctuation-induced tunneling model.[26] The thin non-conductive polymer layers wrapped on the surface of CNTs may act as a barrier for the inter-CNT hopping. The electrical conductivities of the CNT/P3HT nanocomposite films with 20, 30, 40, and 50 wt% CNTs were 8.88 ± 0.55, 50.0 ± 12.2, 162 ± 29, and 224 ± 19 S cm^{-1}, respectively (Fig. 1b). The quantity of CNTs significantly affects the electrical conductivity of the nanocomposite films. As the quantity of CNTs increases, the portion of bare surface of CNTs and the density of the direct junctions between the CNT bundles may increase. Fig. 2c shows the SEM image of the fracture surface of the drop-cast CNT/P3HT nanocomposite film with 50 wt% CNTs. During the fabrication of the fracture surface of the nanocomposite film in liquid nitrogen, the CNT bundles were pulled out from the matrix. A number of flexible CNT bundles were tightly imbedded in the nanocomposite film. Fig. 2d shows the cross-section transmission electron microscope (TEM) image of the drop-cast CNT/P3HT nanocomposite film with 50 wt% CNTs. The cross-section TEM sample was prepared using an *ex situ* lift-out technique with a focused ion beam (FIB). Because of the relatively low electron density of P3HT, the

morphology of the polymer matrix was not identified. The circular and longitudinal cross-sections of the CNTs are clearly visible. The CNTs in the nanocomposite film have 2-4 carbon walls. Thus, the CNTs used in this study were identified as few-walled CNTs.

The few-walled CNT/undoped P3HT nanocomposite films exhibited excellent thermoelectric properties. Recently, we reported that the single-walled CNT/undoped P3HT nanocomposite films exhibited power factors of 86.6 ± 16.2 μW $m^{-1}K^{-2}$.[17] Using the few-walled CNT can be advantageous for obtaining high-performance thermoelectric CNT/conjugated polymers. To compare the thermoelectric properties of the single-walled and few-walled CNTs, we fabricated single-walled and few-walled CNT films on nylon membrane filter disks by vacuum filtration. Because of poor dispersion stabilities, other solution processes cannot be applied. Figs. S3 and S4 shows the AFM and SEM images of the single-walled and few-walled CNT films. The diameters of the CNT bundles and film surface roughness of the CNT films are greater than those of the CNT/P3HT nanocomposite films. The single-walled and few-walled CNT films had similar Seebeck coefficients, i.e., 47 and 51 μV K^{-1}, respectively. The electrical conductivities of the single-walled and few-walled CNT films were 2136 and 3920 S cm^{-1}, respectively. The excellent thermoelectric properties of the few-walled CNT/P3HT nanocomposite films can be originated from the high electrical conductivity of the few-walled CNTs. It was reported that, although the electronic properties of the double-walled CNTs are very similar to those of single-walled CNTs, the electrical conductivity of the double-walled CNTs is higher than that of the single-walled CNTs because of the double-walled CNTs' π conducting channel.[27,28] In this study, the few-walled CNTs with 2-4 carbon walls might exhibit similar phenomena as the double-walled CNTs. The higher electrical conductivity of the few-walled CNTs can also be discussed with the quality of CNTs. Fig. S5 shows the Raman spectra of the single-walled and few-walled CNTs. The D band intensity of

the few-walled CNTs is much smaller than that of the single-walled CNTs. The very low intensity of the D band indicates very low densities of defects and dangling bonds in the few-walled CNTs used in this study. The high quality of few-walled CNTs might be related to their high electrical conductivity.

We found that CNT/P3HT nanocomposite patterns can be spray-printed with a shadow mask (Fig. 3a). Recently, spray-printing attracted much attention as a printing method for creating patterns of active materials in organic electronic and optoelectronic devices.[29-33] Spray-printing is thought to be a simple, fast, low-cost process for large-area organic devices. Spray-printed CNT/P3HT nanocomposite films with 50 wt% CNTs were fabricated, and their thermoelectric properties were evaluated. The thickness of the nanocomposite films was approximately 1 μm. The Seebeck coefficient, electrical conductivity, and power factor of the spray-printed nanocomposite films with 50 wt% CNTs were 97 ± 11 μV K^{-1}, 345 ± 88 S cm^{-1}, and 325 ± 101 μW $m^{-1}K^{-2}$, respectively, at room temperature. When compared with the drop-cast nanocomposite film, the Seebeck coefficient of the spray-printed nanocomposite films was slightly less and the electrical conductivity of the spray-printed nanocomposite films was considerably greater, with a large standard deviation (Table 1). This might be related to the morphology of the nanocomposite films. Figs. 3b and 3c show the AFM and SEM images of the spray-printed CNT/P3HT nanocomposite film with 50 wt% CNTs. The CNT bundles with diameters in the range of 15 – 50 nm in the spray-printed nanocomposite film are more randomly distributed than those in the drop-cast nanocomposite film. The surface root-mean-square roughness values, calculated from the AFM images of the drop-cast and spray-printed nanocomposite films with 50 wt% CNTs were 7.6 nm and 15.5 nm, respectively. In the drop-cast CNT/P3HT nanocomposite film, the CNT bundles were leveled and slightly packed during slow evaporation of the solvent. Because the electrical conductivity of CNTs is much

higher than that of P3HT, the density of the inter-CNT bundle connections is a dominant factor in determining the electrical conductivity of the nanocomposite films. The increased electrical conductivity of the spray-printed nanocomposite films can be because of the higher density of the inter-CNT bundle connections.

Since the spray-printed CNT/P3HT nanocomposite films exhibited excellent thermoelectric properties, a flexible OTEG composed of only p-type CNT/P3HT nanocomposite patterns spray-printed on a polyimide substrate was fabricated (Fig. 4a). The OTEG's 41 p-type active lines, with a width of 1 mm and a length of 15 mm, were connected in series by dispenser-printed silver electrodes (Fig. S6). Fig. 4b shows the output power-output current and output voltage-output current curves of the spray-printed flexible OTEG. A temperature difference of 10 ºC was applied between the two sides of the spray-printed CNT/P3HT lines using two Peltier plates (Fig. S7). The open-circuit voltage, V_o, of the OTEG was measured to be 41.8 mV, which is in close agreement with the calculated value ($V_o = NS\Delta T$, where N is the number of thermoelectric elements) of 39.8 mV. The internal resistance, R_i, was 13.5 kΩ, and the maximum output power, P_{max}, was 32.7 nW, which is very close to the calculated value ($P_{max} = V_o^2/(4R_i)$) of 32.4 nW. For practical applications of spray-printed CNT/P3HT OTEGs, device performance still needs to be improved. By optimizing the device structure and introducing compatible n-type counterparts, the performance of spray-printed OTEGs may be enhanced. This will be our future research topic. In this study, the electrical power generation of the spray-printed OTEG was demonstrated for the first time.

In summary, we reported the fabrication of thermoelectric CNT/P3HT nanocomposite films and a flexible CNT/P3HT OTEG by spray-printing. Within the CNT/P3HT nanocomposite films, few-walled CNT bundles with diameters in the range of 15 – 50 nm formed an interconnected network which is thought to be the electrical pathway. The spray-printed

CNT/P3HT nanocomposite films exhibited excellent thermoelectric properties. The Seebeck coefficient, electrical conductivity, and power factor of the nanocomposite films were 97 ± 11 μV K^{-1}, 345 ± 88 S cm^{-1}, and 325 ± 101 μW $m^{-1}K^{-2}$, respectively. We fabricated a printed flexible OTEG, composed of the pray-printed p-type CNT/P3HT nanocomposite lines and dispenser-printed silver electrode lines, on a polyimide substrate. The electric power generation capability of the OTEG was demonstrated, with a maximum output power of 32.7 nW. Our results suggest that spray-printed thermoelectric organics are promising candidates for flexible, light weight, and low-cost printed OTEGs.

Acknowledgements

This work was supported by a grant from the R&D Convergence Program of the National Research Council of Science & Technology (NST), a grant from the KRICT Core Project (KK-1507-C6), and the Center for Advanced Soft-Electronics funded by the Ministry of Science, ICT and Future Planning as Global Frontier Project (2011-0031628).

Notes and references

1 O. Bubnova, Z. U. Khan, A. Malti, S. Braun, M. Fahlman, M. Berggren and X. Crispin, *Nat. Mater.*, 2011, **10**, 429.

2 G-H. Kim, L. Shao, K. Zhang and K. P. pipe, *Nat. Mater.*, 2013, **12**, 719.

3 G. P. Moriarty, S. De, P. J. King, U. Khan, M. Via, J. A. King, J. N. Coleman and J. C. Grunlan, *J. Polymer. Sci. Part B: Polym. Phys.*, 2013, **51**, 119.

4 C. Bounioux, P. Díaz-Chao, M. Campoy-Quiles, M. S. Martín-González, A. R. Goñi, R. Yerushalmi-Rozen and C. Müller, *Energy Environ. Sci.*, 2013, **6**, 918.

5 Q. Yao, Q. Wang, L. Wang and L. Chen, *Energy Environ. Sci.*, 2014, **7**, 3801.

6 H. Wang, S.-I. Yi, X. Pu and C. Yu, *ACS Appl. Mater. Interfaces*, 2015, **7**, 9589.

7 C. T. Hong, W. Lee, Y. H. Kang, Y. Yoo, J. Ryu, S. Y. Cho and K.-S. Jang, *J. Mater. Chem. A*, 2015, **3**, 12314.

8 C. Yu, K. Choi, L. Yin and J. C. Grunlan, *ACS Nano*, 2011, **5**, 7885.

9 W. Lee, C. T. Hong, O. H. Kwon, Y. Yoo, Y. H. Kang, J. Y. Lee, S. Y. Cho and K.-S. Jang, *ACS Appl. Mater. Interfaces*, 2015, **7**, 6550.

10 B. Endrődi, G. F. Samu, D. Fejes, Z. Németh, E. Horváth, A. Pinsoni, P. K. Matus, K. Hernádi, C. Visy, L. Forró and C. Janáky, *J. Polymer. Sci. Part B: Polym. Phys.*, 2015, DOI:10.1002/polb.23782.

11 Y. Du, S. Z. Shen, W. D. Yang, K. F. Cai and P. S. Casey, *Synth. Met.*, 2012, **162**, 375.

12 Y. Du, K. F. CAi, S. Z. Shen and P. S. Casey, *Synth. Met.*, 2012, **162**, 2102.

13 C. Meng, C. Liu and S. Fan, *Adv. Mater.*, 2010, **22**, 535.

14 Q. Yao, L. Chen, W. Zhang, S. Liufu and X. Chen, *ACS Nano*, 2010, **4**, 2445.

15 Q. Wang, Q. Yao, J. Chang and L. Chen, *J. Mater. Chem.*, 2012, **22**, 17612.

16 J. Chen, X. Gui, Z. Wang, Z. Li, R. Xiang, K. Wang, D. Wu, X. Xia, Y. Zhou, Q. Wang, Z. Tang and L. Chen, *ACS Appl. Mater. Interfaces*, 2012, **4**, 81.

17 W. Lee, C. T. Hong, O. H. Kwon, Y. Yoo, Y. H. Kang, J. Y. Lee, S. Y. Cho and K.-S. Jang, *ACS Appl. Mater. Interfaces*, 2015, **7**, 6550.

18 B. Endrődi, J. Mellár, Z. Gingl, C. Visy and C. Janáky, *RSC Adv.*, 2014, **4**, 55328.

19 S. Ren, M. Bernardi, R. R. Lunt, V. Bulovic, J. C. Grossman and S. Gradečak, *Nano Lett.*, 2011, **11**, 5316.

20 J. Zou, L. Liu, H. Chen, S. I. Khondaker, R. D. McCullough, Q. Huo and L. Zhai, *Adv. Mater.*, 2008, **20**, 2055.

21 T.-A. Chen, X. Wu and R. D. Rieke, *J. Am. Chem. Soc.*, 1995, **117**, 233.

22 X. Ai, N. Anderson, J. Guo, J. Kowalik, L. M. Tolbert and T. Lian, *J. Phys. Chem. B*, 2006, **110**, 25496.

23 Q. Yao, L. Chen, W. Zhang, S. Liufu and X. Chen, *ACS Nano*, 2010, **4**, 2445.

24 K. C. See, J. P. Feser, C. E. Chen, A. Majumdar, J. J. Urban and R. A. Segalman, *Nano Lett.*, 2010, **10**, 4664.

25 A. Thess, R. Lee, R. Nikolaev, H. Dai, P. Petit, J. Robert, C. Xu, Y. H. Lee, S. G. Kim, A. G. Rinzler, D. T. Colbert, G. E. Scuseria, D. Tománek, J. E. Fischer and R. E. Smalley, *Science*, 1958, **273**, 483.

26 E. Kymakis and G. A. J. Amaratunga, *J. Appl. Phys.*, 2006, **99**, 084302.

27 J. Q. Wei, H. W. Zhu, B. Jiang, I. J. Ci and D. H. Wu, *Carbon*, 2003, **41**, 2495.

28 Y. Ryu, D. Reeman and C. Yu, *Carbon*, 2011, **49**, 4745.

29 D. Vak, S.-S. Kim, J. Jo, S.-H. Oh, S.-I. Na, J. Kim and D.-Y. Kim, *Appl. Phys. Lett.*, 200 7, **91**, 081102.

30 K. X. Steirer, M. O. Reese, B. L. Rupert, N. Kopidakis, D. C. Olson, R. T. Collins and D. S. Ginley, *Sol. Mater. So. Cells*, 2009, **93**, 447.

31 C. K. Chan, L. J. Richter, B. Dinardo, C. Jaye, B. R. Conrad, H. W. Ro, D. S. Germack, D. A. Fischer, D. M. DeLongchamp and D. J. Gundlach, *Appl. Phys. Lett.*, 2010, **96**, 133304.

32 D. Khim, K.-J. Baeg, B.-K. Yu, S.-J. Kang, M. Kang, Z. Chen, A. Facchetti, D.-Y. Kim and Y.-Y. Noh, *J. Mater. Chem. C*, 2013, **1**, 1500.

33 A.-N. Cha, Y. Ji, S.-A. Lee, Y.-Y. Noh, S.-I. Na, S. Bae, S. Lee and T.-W. Kim, *Mater. Sci. Eng. B*, 2015, **191**, 51.

Figures and Table

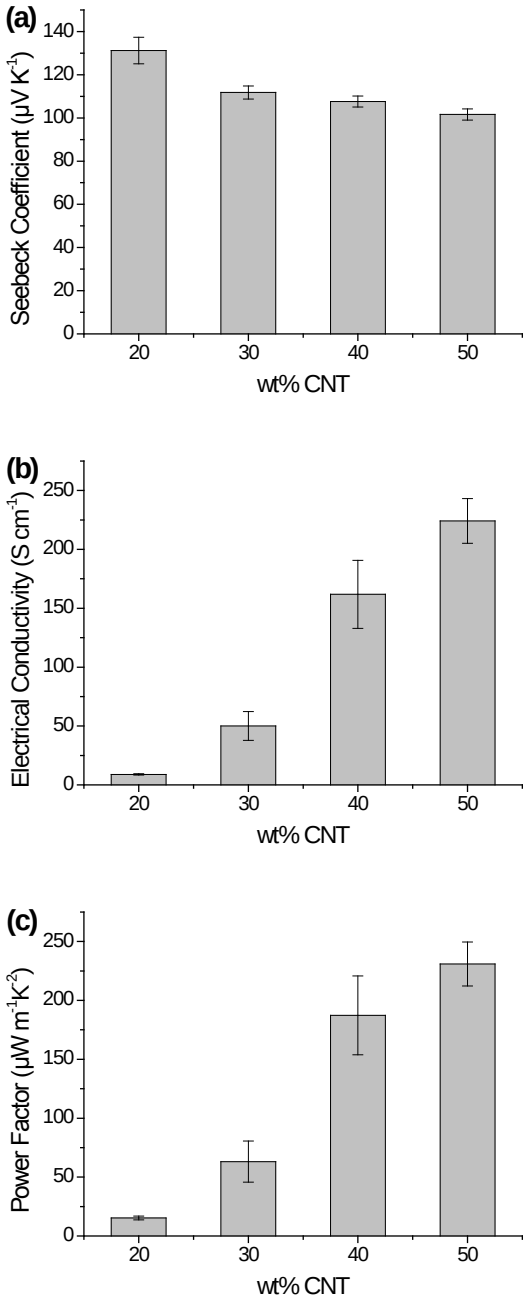

Fig. 1 Dependence of the (a) Seebeck coefficient, (b) electrical conductivity, and (c) power factor on the quantity of CNTs in drop-cast CNT/P3HT nanocomposite films.

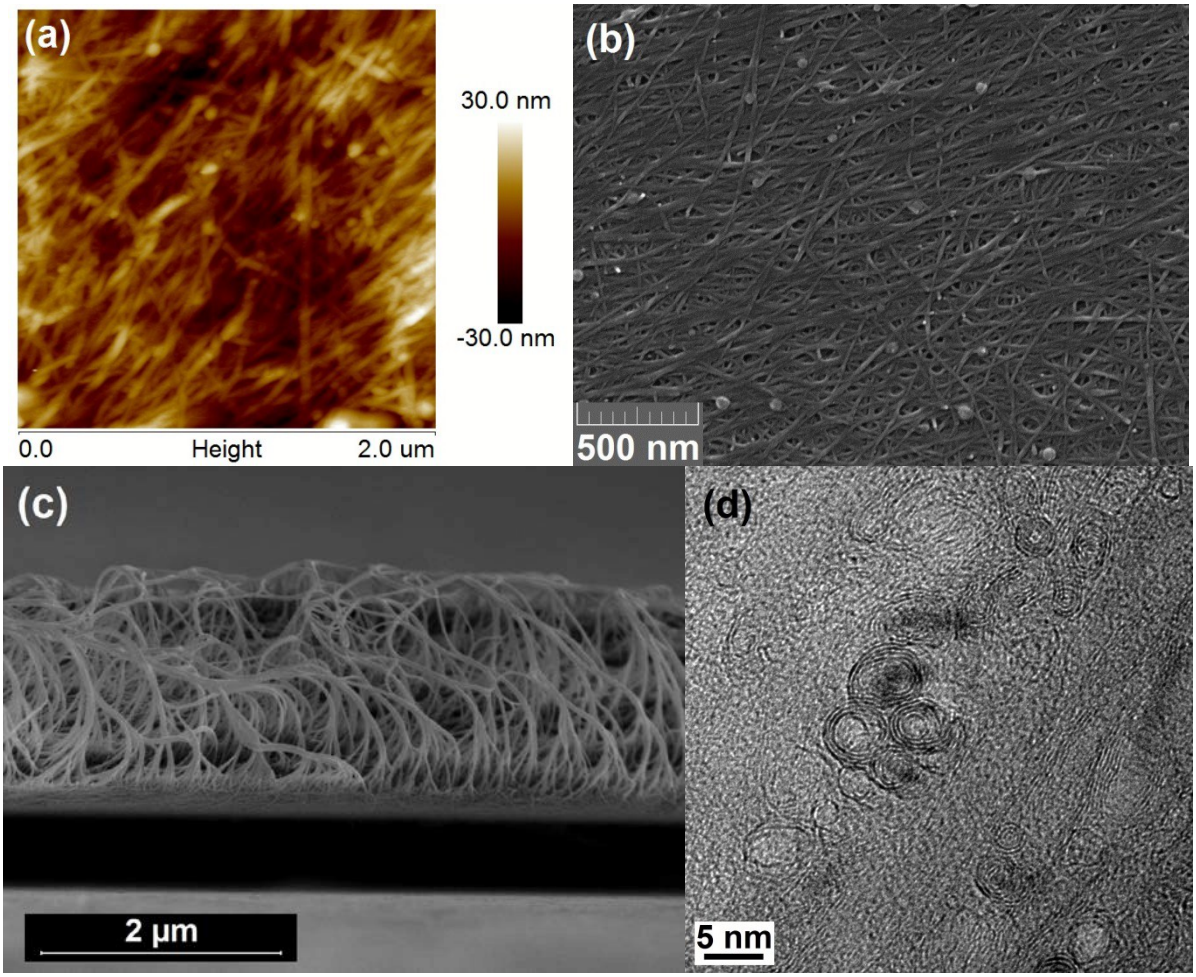

Fig. 2 (a) AFM, (b) SEM, (c) fracture-surface SEM, and (d) cross-section TEM images of the drop-cast CNT/P3HT nanocomposite films with 50 wt% CNTs.

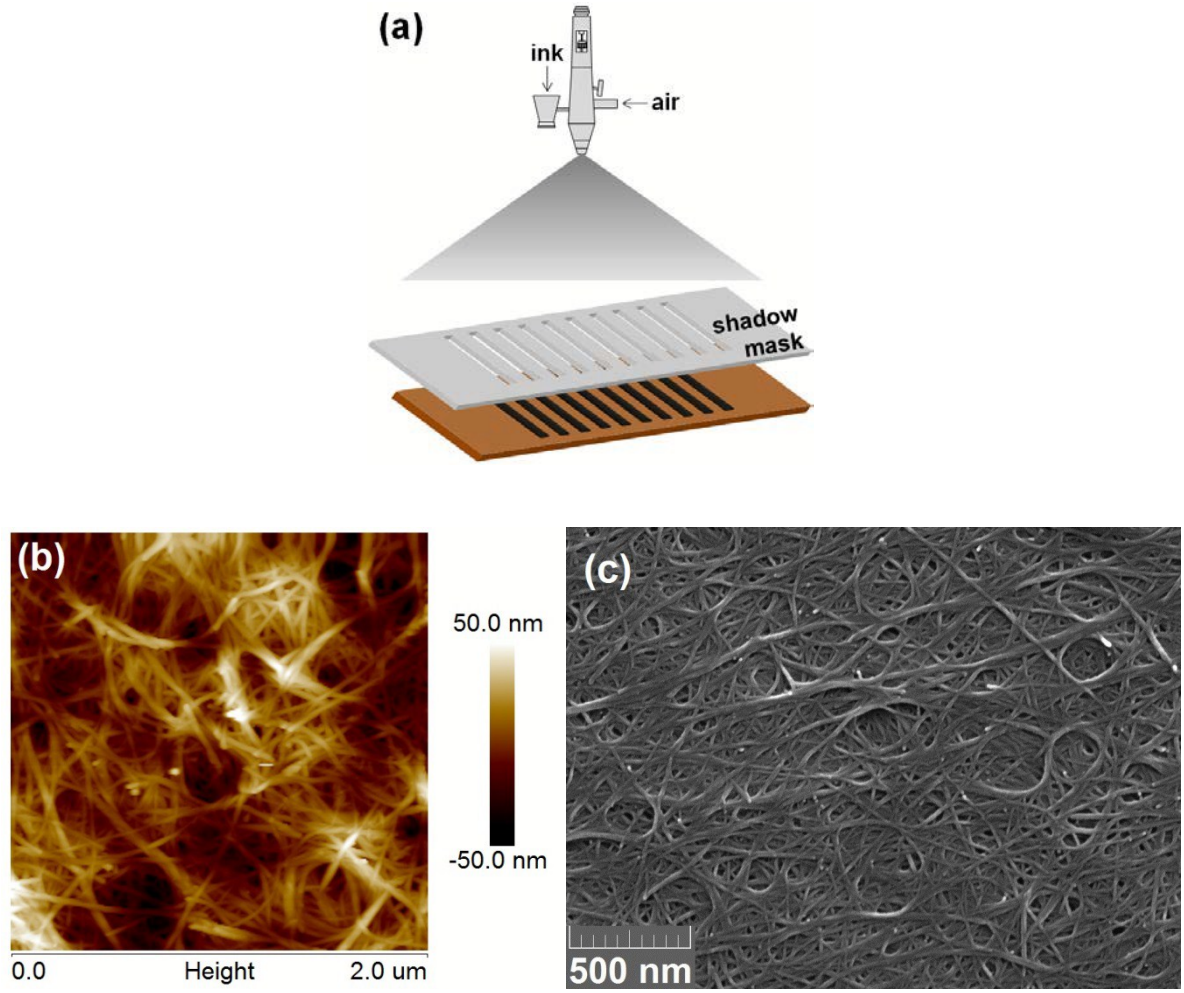

Fig. 3 (a) Schematic drawing of the spray-printing process, and (b) AFM and (c) SEM images of spray-printed CNT/P3HT nanocomposite films with 50 wt% CNTs.

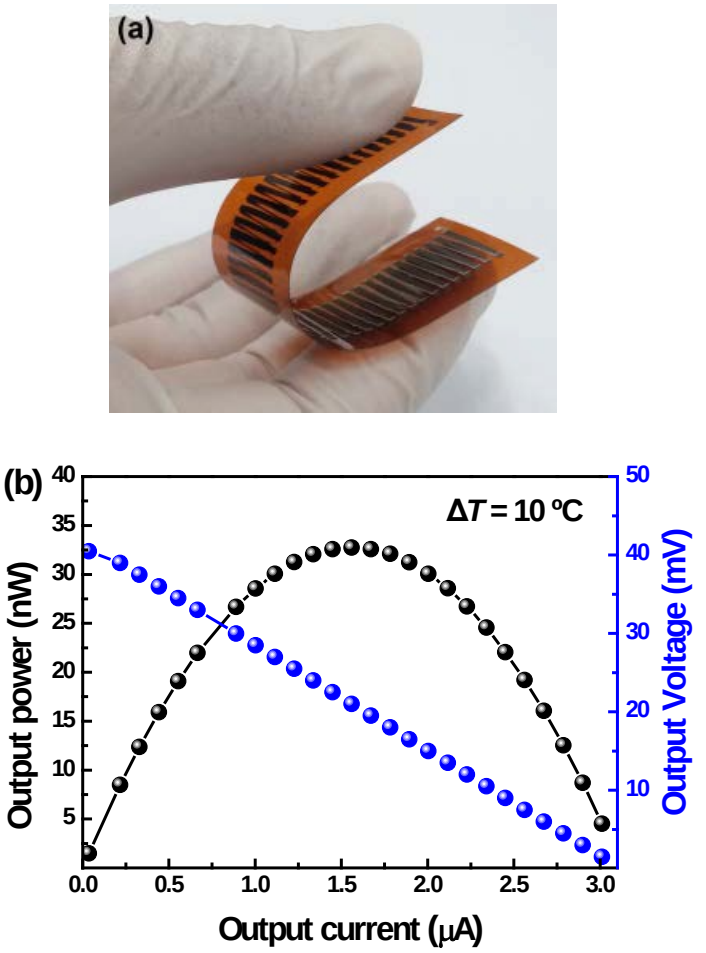

Fig. 4 (a) Photograph and (b) output power-output current and output voltage-output current curves of the spray-printed flexible CNT/P3HT OTEG.

Table 1 Thermoelectric properties of drop-cast and spray-printed CNT/P3HT films with 50 wt% CNTs

Coating method	Seebeck coefficient [μV K^{-1}]	Electrical conductivity [S cm^{-1}]	Power factor [μW $m^{-1}K^{-2}$]
Drop-casting	102 ± 3	224 ± 19	231 ± 19
Spray-printing	97 ± 11	345 ± 88	325 ± 101

We report the fabrication of high-performance thermoelectric carbon nanotube/poly(3-hexylthiophene) (CNT/P3HT) nanocomposite films and flexible CNT/P3HT organic thermoelectric generators by spray-printing.